
Article:
Jiang, S, Ye, Y, Tan, Y et al. (4 more authors) (2018) Discrete element simulation of particle motion in ball mills based on similarity. Powder Technology, 335. pp. 91-102. ISSN 0032-5910

https://doi.org/10.1016/j.powtec.2018.05.012

Discrete element simulation of particle motion in ball mills based on similarity

Shengqiang Jiang[a,*], Yixuan Ye[a], Yuanqiang Tan[b], Sisi Liu[a], Jingang Liu[a], Hao Zhang[c], Dongmin Yang[d,*]

a. School of Mechanical Engineering, Xiangtan University, Xiangtan, 411105, China

b. Institute of Manufacturing Engineering, Huaqiao University, Xiamen, 361021, China

c. School of Metallurgy, Northeastern University, Liaoning, 110819, China

d. School of Civil Engineering, University of Leeds, LS2 9JT, UK

Abstract: Discrete element (DE) simulation of a ball mill with a large number of particles is challenging when each particle is considered. Similarity principle could be adopted to reduce the number of particles in a simulation whilst still maintaining the accurate flow behaviour of particles. This paper presents a scaling relationship between particle gravitational acceleration, mill diameter and mill rotational speed. A series of scaled simulations of particle motion with different mill diameters are carried out. Consistent motion of a single particle and multiple particles in ball mills with different diameters and rotational speeds verifies the proposed relationship, which could be an effective approach to reduce the size of simulations for ball mills.

Key words: similarity principle; ball mill; particle motion; discrete element method

1. Introduction

Rotating drums have been widely employed in chemical, cement, mineral and pharmaceutical industries. Ball mill is a type of rotating drum, mainly used for grinding and the particle motion in a ball mill is a major factor affecting its final product. However, understanding of particle motion in ball mills based on the present measurement techniques is still limited due to the very large scale and complexity of the particle system. Quantitative information, such as particle distributions and energy change, is still difficult to obtain through experiments. Thus, computer-based numerical methods have been proposed to further investigate the particle motion in a ball mill.

As one of the main particle-based methods, the discrete element method (DEM) was first proposed by Cundall [1] in 1979 to simulate the rock fracture problem. DEM is based on Newton's second law to track the movement of each particle in the particle assembly and simulate the collision of between particles. It has been successfully applied to soil [2, 3], rock [4], powder [5-7] and other bulk materials for particle movement analysis and ceramic [8-10], concrete [11, 12] and other brittle materials for crushing and crack propagation simulations. Although the DEM has provided useful results in the simulation of particle flow behaviour, it requires extremely large computer capacity as the numerical model

* Corresponding authors. Tel: +86 731 58292225
E-mail address: jsqcx@xtu.edu.cn (S. Jiang); d.yang@leeds.ac.uk (D. Yang)

reaches to a level of tens of millions of particles in three dimensions. As an attempt to address this large scale issue, Feng and Owen [13] proposed a scale classification method by the number of particles, such as micro-scale ($<10^6$), meso-scale (10^6~10^9) and macro-scale ($>10^9$). Micro-scale problems with less than several million particles have been modeled by DEM. However, real industrial applications may involve billions of particles as classified as macro-scale, such as a ball mill, rotary dryer, crusher, etc. DEM has been used to interpret the movement of particles and improve the operation and production of rotating drum in the last two decades. Finnie et al. [14] cited the scaling relationship for rotating drums derived from Ding et al. [15] and used DEM to simulate the process of particle movement in horizontal rotary kiln and analyzed the longitudinal and transverse particles when including filling rate and speed. Siiria et al. [16] studied the mixing process of powder and tracked the trajectories of the kinematic roots of each particle using DEM; furthermore, the authors analyzed and compared the average energy of each particle simulation system. The DEM results from the above studies helped to improve the understanding of the movement law of the particles and optimization of the equipment geometry and operation parameters.

A number of researchers have reported their simulation strategies for rotating drums in the literature, as enumerated in Table 1. For the sake of reducing the scale of the calculation, suggested ways are reducing the size of the model and the filling rate [17-23]. However, industrial rotating drums are much larger than the aforementioned studies and a detailed study on the specific effects of scaling model is still absent. Powell et al. [24] simulated a short slice of the mill thus the number of balls was reduced from 4.5 million to 110 thousand resulting in a reduction of simulation time by at least 50-fold. From the above reference survey, it is found that most of the DEM simulations are very different to the real mill systems and thus it is difficult to use DEM to deal with all the particles in a real mill, even with graphics processing unit (GPU) computing [25-27], parallel computing [28, 29], continuum approximation [30, 31], etc. Modern GPUs are very efficient at manipulating computer graphics and image processing, and their highly parallel structure makes them more efficient than general-purpose CPUs for algorithms where the processing of large blocks of data is done in parallel. Ge et al. [25, 26] adopted GPU to accelerate the numerical simulation in which quasi-real-time simulation is reached. Parallel computing can speed up DEM simulations and may be the most powerful solution. Using parallel computing or GPU computing to accelerate the calculation is a very attractive method, but it needs a good computer configuration as support. Continuum mechanics may be applied to both discrete and heterogeneous media through the use of homogenization theory, which provides a mathematically elegant and rigorous framework for replacing a discrete collection of interacting entities by an equivalent homogenous continuum. The use of the continuum mechanics method may be difficult to capture a variety of physical particle information from the micro-scale, and it is difficult to analyse the relationship between the particle forces.

Table 1 Summary of simulation work about rotating drums.

Reference paper	Drum diameter（mm）	Ball diameter (mm)	Ball number (maximum)	Filling rate (by volume)	Particle scale	DEM platform
[14]			21333	0.2~0.4	Micro-scale	2D
[17]	1120	40~190		0.2~0.3	Micro-scale	3D
[18]	125	3~5	5208	0.1	Micro-scale	3D
[19]	254/381/900	15.2		0.4~0.24	Micro-scale	3D
[20]	70	1.3	47000	0.3~0.92	Micro-scale	3D
[21]	573	8~20	14431	0.35	Micro-scale	3D(EDEM)
[22]	1696	31~88	14164	0.18	Micro-scale	3D(EDEM)
[23]	198	2.4	5400	0.107	Micro-scale	3D
[24]	8000	18.8~53	109956	0.4	Micro-scale	3D(EDEM)
[25]	100~210	1~7	184608	0.35	Micro-scale	3D(GPU)
[26]	1500	10	9606450		Meso-scale	3D(GPU)

The present work aims to attempt the huge particle computing system problem and simulation difficulty. Firstly, the motion and force states of particles in the ball mills will be analysed according to the force balance principle. A series of conversion formulas for the mill's structural and kinematic parameters based on centrifugal force are derived. Then, six sets of three-dimensional DEM models of ball mills are established, where the movement of single particle and multi particles is numerically simulated, respectively. The conversion formulas are validated by simulation results of single particle in terms of the motion trajectories and energy change. In addition, particle motion and mass flow of multiple particles is investigated in detail to further verify the above formulas.

2 Scaling theory

2.1 Force Balance of Particles in the Ball mills

The movement of the particulate materials in the ball mills is closely related to the rotational speed of the mill. With the increase of rotational speed of the mill, the movement of the particulate materials mainly undergoes slipping, cataracting and centrifuging [32], as shown in Fig. 1. In a ball mill, the grinding media (steel balls) are attached to the mill liner due to inertial and centrifugal forces when the mill starts to rotate. Then, the grinding media move to a certain height and are thrown under gravity. After throwing the grinding media crush the particulate materials within the ball mills to achieve comminution.

Fig. 2 shows a kinematic trajectory model of the particle throwing process in the mill, where the throwing movement has a significant influence on the efficiency of the ball mill. By retrieving a certain particle in the outermost layer of the ball mills, the motion trajectories of the particle at different time during the process of dropping can be analyzed. As

shown in Fig. 2, R is the radius of ball mills; point A is the particle detachment point; α is the detaching angle (angle between OA and the vertical direction); ω is the rotational speed of mill, and t_0-t_5 is the different time points in the motion trajectory. When the outer particle is located at point A, the vertical component of the centrifugal force of the particle is equal to the gravity but in the opposite direction. Assuming the particle is a mass point and ignoring the role of friction, we have:

$$F = mg\cos\alpha \tag{1}$$

where F is the centrifugal force (scalars), m is the mass of the particles, g is the gravitational acceleration, and α is the detaching angle. Then, based on centrifugal force calculation formula, F can be written as:

$$F = mv^2/R = mR\omega^2 \tag{2}$$

where v is the velocity of the particle, R is the radius of the ball mill, and ω is the rotational speed of the mill.

Combining Eqs. (1) and (2) gives the following:

$$\omega = \sqrt{\frac{g}{R}\cos\alpha} \tag{3}$$

And the detaching angle of the particles can be calculated as:

$$\alpha = \arccos\frac{R\cdot\omega^2}{g} \tag{4}$$

From the above equations, it can be seen that the detaching angle is dependent on the rotational speed of the mill as well as the radius of ball mill and the gravitational acceleration.

2.2 Model scaling

Due to the large size of a ball mill or a rotary kiln, the number of particles is massive. Therefore, it is difficult to build a DEM model to include all the particles of real size in a mill with real geometry. Fig. 3 shows a ball mills with a radius of 3.9 m and a width of 1 m. If the particle radius is identical to 20 mm, then the number of particles would reach 278,058 to achieve a 30% filling rate. However, when the radius of the ball mills is scaled down to 1 m, the corresponding width of the ball mills becomes 256 mm and the number of particles is proportionally reduced to 4,680 at the same filling rate of 30%. It can be seen that a scaling down of the size of the mill can greatly reduce the size of the particle system and improve the computational efficiency. However, it is important to ensure that the scaled model still produces accurate simulation of particles motion as the original physical model. In this regard, a scaled test is often used in engineering practice [33, 34]. In general, the scaled model first needs to have geometrical similarity in configuration, and the scaled coefficient of the physical parameters should be based on similar criteria of force or other physical quantities. In this study, the particle size is kept unchanged but the radius of ball mill is reduced. Based on the force similarity principle [13, 35], the relationship between the structural, motion, force and energy parameters of the physical

and the scaled models can be established. In order to ensure that the particle motion in the scaled model and the physical model are similar, the detaching angles in the two models must be equal, i.e.,

$$\alpha^{S} = \alpha^{P} \tag{5}$$

where α^{P} and α^{S} are the detaching angle in the physical model and the scaled model, respectively. Combing Eqs. (4) and (5) gives:

$$\arccos\frac{R^{S}\cdot\left(\omega^{S}\right)^{2}}{g^{S}} = \arccos\frac{R^{P}\cdot\left(\omega^{P}\right)^{2}}{g^{P}} \tag{6}$$

where ω^{P} and ω^{S} are the rotational speed of mill in the physical model and scaled model, respectively; g^{P} and g^{S} are the gravitational acceleration in the physical model and scaled model, respectively; R^{P} and R^{S} are the mill radius in the physical model and scaled model, respectively.

S is define as the scaling factor of the radius ratio between the two models as:

$$S = \frac{R^{P}}{R^{S}} \quad (S \geqslant 1) \tag{7}$$

or

$$S = \frac{h^{P}}{h^{S}} \quad (S \geqslant 1) \tag{8}$$

Accordingly, Eq. (6) can be reformulated as:

$$\frac{\left(\omega^{S}\right)^{2}}{g^{S}} = \frac{S\cdot\left(\omega^{P}\right)^{2}}{g^{P}} \tag{9}$$

If the gravitational acceleration in the physical model and scaled model are equal ($g^{S} = g^{P}$), ω^{S} can be calculated as:

$$\omega^{S} = \sqrt{S}\omega^{P} \tag{10}$$

Thus the rotation speed of the mill in the scaled model needs to be $\sqrt{S}$ times that of the physical model.

Alternatively, if the rotational speed of mill in the physical model and scaled model are equal ($\omega^{S} = \omega^{P}$), g^{S} can be calculated as:

$$g^{S} = g^{P} / S \tag{11}$$

Thus the gravitational acceleration in the scaled model needs to be reduced to 1/S times the physical model.

2.3 Energy conversion

The working principle of rotary cylinder type devices such as a ball mill is that the grinding media moves to a certain height with the ball mill. Then the media falls under the influence of gravity and crushes the material in the mill. Therefore, the law of energy variation in the material falling process can be established, and the equivalence of the scaled model can be verified. Based on the law of energy conservation, the change of kinetic energy and the change of potential energy are equal in the process of falling, denoted as $|\Delta E|$ which is calculated by:

$$|\Delta E| = \frac{1}{2} m v_b^{\,2} - \frac{1}{2} m v_a^{\,2} = mgh_b - mgh_a \tag{12}$$

where v_a and v_b are the velocities at any two points a and b in the particle's falling process, respectively; h_a and h_b are the height at any two points a and b in the particles falling process, respectively.

Combing Eq. (8) and Eq. (12), we have:

$$|\Delta E|^P = mg^P (h_b^{\,P} - h_a^{\,P}) = Smg^S (h_b^{\,S} - h_a^{\,S}) \quad (\text{if } g^S = g^P) \tag{13}$$

and combing Eqs. (8), (11) and (12), we have:

$$|\Delta E|^P = mg^P (h_b^{\,P} - h_a^{\,P}) = S^2 mg^S (h_b^{\,S} - h_a^{\,S}) \quad (\text{if } \omega^S = \omega^P) \tag{14}$$

where $|\Delta E|^P$ is the change of energy between any two points a and b of the particle throwing process in the physical model; $h_a^{\,P}$, $h_b^{\,P}$ is the height of the different positions of the ball mill in the physical model; $h_a^{\,S}$, $h_b^{\,S}$ is the corresponding height of the different positions of the ball mill in the scaled model.

If we denote $|\Delta E|^S = mg(h_b^{\,S} - h_a^{\,S})$, then

$$\frac{|\Delta E|^S}{|\Delta E|^P} = 1/S \qquad (\text{if } g^S = g^P) \tag{15a}$$

$$\frac{|\Delta E|^S}{|\Delta E|^P} = 1/S^2 \qquad (\text{if } \omega^S = \omega^P) \tag{15b}$$

This indicates that when the gravitational acceleration in the scaled model is kept constant, the change of energy of the particles falling in the scaled model is 1/S of the physical model; when the rotational speed of mill in the scaled model is kept constant, the change energy of the particles falling in the scaled model is $1/S^2$ of the physical model. According to the above calculations, the ratios of the physical quantity in the scaled model to those in the physical model are listed in Table 2.

Table 2 Scaling factors for the physical quantities.

Simulation Parameters	λ_1	λ_2

Radius of ball mill R	1/S	1/S
Height of particle position h	1/S	1/S
Gravitational acceleration g	1	1/S
Rotational speed of mill ω	$\sqrt{S}$	1
Energy change ΔE	1/S	$1/S^2$

Note that λ_1 is the scale factor representing the ratio of the physical quantity in the scaled model to the physical quantity in the physical model when g is constant, and λ_2 is the scale factor representing the ratio of the physical quantity in the scaled model to the physical quantity in the physical model when ω is constant.

3 Numerical simulations

3.1 Discrete element method

The DEM is a numerical method to address the kinematic and mechanical behaviour of complex granular systems involving many discrete units with certain shapes and masses. It has been widely used in ball mills [18, 36] to determine the particles behaviour and the torque and energy of ball mills in different working conditions. In DEM each particle is tracked and its motion is governed by Newton's second law:

$$\text{Translational motion} \quad m\frac{dV_i}{dt} = F_i - \beta_g V_i \tag{16}$$

$$\text{Rotational motion} \quad I\frac{d\omega_i}{dt} = M_i - \beta_g \omega_i \tag{17}$$

where i (=1, 2, 3) denotes the x, y and z coordinate directions, respectively; F_i is the out-of-balance force component of the particle; V_i is the translational velocity; m is the mass of the particle; M_i is the out-of-balance moment due to the contacts; ω_i is the rotational velocity; I is the rotational inertia of the particle; β_g is the global damping coefficient; dt is the time step.

The particle-particle interaction is determined by contact models in DEM. In this study, the Hertz-Mindlin contact model is used to describe the particle-particle and particle-wall collisions, as shown in Fig. 4. In Hertz-Mindlin no-slip model, the normal contact forces between particle a and particle b can be described as the function of normal overlap δ_n [37, 38]:

$$F_n^c = \frac{4}{3} E^* \sqrt{R^*} \delta_n^{3/2} \tag{18}$$

Where E^* is the equivalent Young's Modulus and R^* is the equivalent radius.

The normal damping forces is described as:

$$F_n^d = -2\sqrt{\frac{5}{6}}\beta\sqrt{S_n m^*}\,v_n^{\overline{rel}} \tag{19}$$

Where m^* is the equivalent mass, β is the damping ratio, S_n is the normal stiffness, and $v_n^{\overline{rel}}$ is the normal relative velocity between contact element a and b.

The tangential contact forces between particle a and particle b depends on the tangential overlap δ_t and the tangential stiffness S_t [37-39]:

$$F_t^c = -S_t\delta_t \tag{20}$$

The tangential damping force is described as:

$$F_t^d = -2\sqrt{\frac{5}{6}}\beta\sqrt{S_t m^*}\,v_t^{\overline{rel}} \tag{21}$$

where $v_n^{\overline{rel}}$ is the tangential relative velocities between contact element a and b.

The tangential force is limited by Coulomb friction according to $F_t^c < \mu_s F_n^c$.

Rolling friction is accounted for by applying a torque to the contacting surfaces

$$T^i = -\mu_r F_n^c R_i \omega_i \tag{22}$$

Where μ_s and μ_r are the coefficient of static and rolling friction, R_i is the distance of the contact point from the center of mass for the object, and ω_i is the unit angular velocity vector of the object at the contact point. The coefficients in Eqs. (18-22) are given in Table 3.

Table 3 Spring stiffness and damping coefficients used in the contact model.

	Normal direction	**Tangential direction**
Spring stiffness constant (K)	$K_n = \frac{4}{3}E^*\sqrt{R^*\delta_n}$	$K_t = 8G^*\sqrt{R^*\delta_n}$
Damping coefficient (C)	$C_n = 2\sqrt{\frac{5}{6}}\beta\sqrt{S_n m^*}$	$C_t = 2\sqrt{\frac{5}{6}}\beta\sqrt{S_t m^*}$
Stiffness (S)	$S_n = 2E^*\sqrt{R^*\delta_n}$	$S_t = 8G^*\sqrt{R^*\delta_n}$
Equivalent Young's Modulus	$\frac{1}{E^*} = \frac{1-\gamma_a^2}{E_a} + \frac{1-\gamma_b^2}{E_b}$	
Equivalent mass,	$\frac{1}{m^*} = \frac{1}{m_a} + \frac{1}{m_b}$	
Equivalent radius	$\frac{1}{R^*} = \frac{1}{R_a} + \frac{1}{R_b}$	

Damping ratio	$\beta = \frac{\ln e}{\sqrt{\ln^2 e + \pi^2}}$

Where e is the coefficient of restitution, and G^* is the equivalent shear modulus.

3.2 DEM model of the ball mill

Fig. 5 shows a DEM model of the physical ball mill (the radius is 3.9 m, and the length is 1 m) and five scaled models of the ball mill; there are 25 lifters fixed on the inner wall of the mill. The two ends of the mill are set as the periodic boundary. The structural parameters of ball mill and scaled model are shown in Table 4, wherein R is the major diameter of the ball mill, r is the minor diameter of the ball mill, D_1 is the width of the top of the lifters, and D_2 is the distance between two adjacent lifters. The parameters of the particles and the ball mill, as well as the interaction parameters of particles-particle and particles-ball mill wall are shown in Table 5.

Table 4 Geometry parameters of the ball mill in DEM models.

Parameter	Physical Model	Scaled Models
R (mm)	3900	3600/3300/3000/2300/1500
r (mm)	3610	3332/3055/2777/2129/1388
D_1 (mm)	250	231/212/192/147/96
D_2 (mm)	635	586/537/488/374/244
L (mm)	1000	923/846/769/590/385

Table 5 Parameters used in DEM simulations.

Parameter	Value
Radius of particle R_i (mm)	20
Density of particle ρ_i (kg/m$^{3)}$	2678
Filling rate η (% volume)	30
Time of simulation T (s)	20
Porosity n	0.35
Poison ratio υ	0.3
Shear modulus G (pa)	2.3×10^7
Density of mill **ρ_d (kg/m$^{3)}$**	7680
Static friction coefficient of particle-particle μ_1	0.545
Static friction coefficient of particle-wall μ_2	0.5
Rolling friction coefficient of particle-particle m_{r1}	0.01

Rolling friction coefficient of particle-wall m_{r2}	0.01
Restitution coefficient of particle-particle e_1	0.1
Restitution coefficient of particle-wall e_2	0.2

196

197 3.3 DEM simulations of ball mills

198 To verify the accuracy of the formula proposed above, a physical model and five scaled models of ball mills are
199 built using the EDEM software (DEM Solutions Ltd., UK). The detaching angles and the energy conservation by
200 observing the trajectories of a single particle in the ball mill in all models are compared and verified. However, any single
201 particle cannot move freely without colliding with others inside a ball mill, and an actual industrial mill always has a
202 huge number of particles. Therefore, the simulation of a single particle cannot fully explain the problem of particle
203 motion. Further verifications for multiple particles must be completed. In the single particle simulation, the radius of
204 particles in all models is 20 mm and the mass of the particle is 0.089 kg. In the simulations of multiple particles, the
205 number of particles (the radius of the particle is normal distribution, the average particle size is 20 mm) will be generated
206 according to a filling rate of 30%. The motion of the particles will be observed at different times. The following two
207 schemes are used for the simulations:

208 (1) Setting the gravitational acceleration g = 9.81 m/s^2, the rotational speed of the mill after scaling is then
209 calculated according to Eq. (10). The physical parameters and scale coefficients are chosen according to Table 6.

210 (2) Setting the rotational speed of mill ω=1 rad/s, the gravitational acceleration after scaling is calculated according
211 to Eq. (11). The physical parameters and scale coefficient are chosen according to Table 7.

212 **Table 6** Physical parameters in each model with identical gravitational acceleration.

Parameter	Physical model	Scaled model 1	Scaled model 2	Scaled model 3	Scaled model 4	Scaled model 5
Radius of ball mill (m)	3.9	3.6	3.3	3.0	2.3	1.5
Gravitational acceleration (m/s^2)	9.81	9.81	9.81	9.81	9.81	9.81
Rotational speed of mill (rad/s)	1.00	1.04	1.09	1.14	1.30	1.61
Frouder number	0.40	0.40	0.40	0.40	0.40	0.40
Total mass of particles (kg) (single particle / multiple particles)	0.089/2.06×10^4	0.089/1.62×10^4	0.089/1.34×10^4	0.089/8.97×10^3	0.089/4.49×10^3	0.089/1.19×10^3
Scale coefficient	1.000	1.083	1.182	1.300	1.696	2.600

213 **Table 7** Physical parameters in each model with identical mill rotational speed.

Parameter	Physical model	Scaled model 1	Scaled model 2	Scaled model 3	Scaled model 4	Scaled model 5
Radius of ball mill (m)	3.9	3.6	3.3	3.0	2.3	1.5
Gravitational acceleration (m/s^2)	9.81	9.06	8.30	7.55	5.78	3.77
Rotational speed of mill (rad/s)	1.00	1.00	1.00	1.00	1.00	1.00
Frouder number	0.40	0.40	0.40	0.40	0.40	0.40
Total mass of particles (kg) (single particle / multiple particles)	$0.089/2.06\times10^4$	$0.089/1.62\times10^4$	$0.089/1.34\times10^4$	$0.089/8.97\times10^3$	$0.089/4.49\times10^3$	0.089/1.19×103
Scale coefficient	1.000	1.083	1.182	1.300	1.696	2.600

4 Results and discussion

4.1 Single particle

The motion trajectories of the single particle in the physical model and the five scaled models are shown in Fig. 6. The origin of the coordinate system is the center of the ball mill. Figs. 6(a) and 6(b) show the trajectories of the particle under different rotating speeds (set g = 9.81 m/s^2) and different gravitational acceleration (set ω = 1 rad/s), respectively. It can be seen that the particle is generated at the bottom of the mill in Fig. 6. When the mill starts to rotate, the particle rises up with the ball mill until it is thrown out, and the trajectory of the process is parabolic. Then, the particle hits with the mill wall, resulting in rebound until it is balanced. The particle then rises up again with the ball mill and a new cycle starts. From Fig. 6, it can be concluded that the trajectories of the particle in the scaled model are consistent with that in physical model and the detaching angles in each model are approximately 68°.

To verify the energy relationship between the scaled model and the physical model, the energy change of the single particle in each model is monitored, and the energy change curves of the six models are shown in Fig. 7.

In general the energy change curves can be divided into four regions. In region I, the particle is formed at the middle bottom in the ball mill. The particle collides with the mill wall and rebounds slightly when the rotating starts. Therefore, the kinetic energy curve suddenly jumps at the moment of collision, and disorderly fluctuation appears due to the rebound of the particle. The potential energy curve is parabolic because of particle rebound. In region II, the particle reaches equilibrium and then rise up with mill rotation. Hence, the kinetic energy is relatively low, and the potential energy curve gradually increases as the particle position increases. In region III, the particle moves to the detaching point (point A in Fig. 6), and the particle starts to detach from the mill wall and is thrown out. The particle then continues to rise up to the highest position until it touches the mill upon falling. Therefore, the kinetic energy curve shows a slightly downward trend. The potential energy curve continues to rise, reaching the maximum value when the particle moves to

the highest position (t_1 in Fig. 6), and then decreases when the particle drops. In region IV, the particle collides with the ball mill, resulting in rebounding; hence, disorderly fluctuations appear in the kinetic energy curve. The ups and downs appear in the potential energy curve several times due to the particle rebounds. Then, the energy curve goes into region II again, and the next cycle begins.

From Fig. 7, it can be seen that the kinetic energy change curve obtained in the two schemes is approximately parabolic upward in the particle throwing stage. The potential energy change curve is a parabola with a downward opening; when one curve is rising, the other is falling. To further study the energy change law of the physical and the scaled models, the energy data of the two corresponding positions of the particle throwing process in the six simulation models are extracted. The change of kinetic energy and potential energy are obtained. If the gravitational acceleration was set to 9.81 m/s^2 and the rotational speed of mill is changed (see Table 6), the energy change data between the two points of θ_a (2.591 rad) and θ_b (3.568 rad) in Fig. 7 are extracted as shown in Table 8. If the rotational speed of the mill was set to 1 rad/s and the gravitational acceleration is changed (see Table 7), the energy change data between the two points of θ_c (2.580 rad) and θ_d (3.570 rad) in Fig. 7 are extracted as shown in Table 9. The energy change ratio figure is drawn based on the data in Tables 8 and 9, as shown in Fig. 8. It can be seen that the ratio of the energy change in the scaled model to the energy change in the physical model is linear with 1/S at different rotational speeds (Correlation coefficient of 0.998), and the ratio of the energy change in the scaled model to the energy change in the physical model is squared with 1/S at different gravitational acceleration (Correlation coefficient of 0.996). This is consistent with the Eq. (15) derived above.

Table 8 Values of energy change (change rotational speed of the mill).

Parameters	Physical model	Scale model 1	Scale model 2	Scale model 3	Scale model 4	Scale model 5
Radius of mill (m)	3.9	3.6	3.3	3.0	2.3	1.5
Energy change |ΔK| (J)	4.57	4.22	3.79	3.44	2.70	1.77
1/S	1.000	0.923	0.846	0.769	0.589	0.385
Actual ratio	1.000	0.922	0.830	0.753	0.591	0.387

Table 9 Values of energy change (change the gravitational acceleration).

Parameters	Physical model	Scale model 1	Scale model 2	Scale model 3	Scale model 4	Scale model 5
Radius of mill (m)	3.9	3.6	3.3	3.0	2.3	1.5
Energy change |ΔK| (J)	4.39	3.76	3.15	2.61	1.55	0.66
1/S^2	1.000	0.852	0.716	0.592	0.348	0.148
Actual ratio	1.000	0.856	0.718	0.594	0.353	0.151

4.2 Multiple particles

The simulation results of a single particle show that the overall motion of a single particle in the scaled model can be consistent with that in the physical model by changing the rotational speed of the mill or the gravitational acceleration. However, for practical industrial applications wherein the number of particles is huge, the simulation of a single particle cannot fully explain the problem of particle motion. Therefore, simulations of multiple particles are essential. According to the parameters shown in Tables 6 and 7, six simulation models are established. The comparison of the entire particle motion morphology in different simulation models at different times is examined, as shown in Figs. 9 and 10. To better compare the particle motion, the particles in Figs. 9 and 10 initially coloured in red and blue before the ball mill begins to move. The surface contour data of the particles in those six scaled models at different time intervals are extracted and plotted in Fig. 11. Combining Figs. 9, 10, and 11, the general particle motion during the throwing process in different simulation models is consistent. Notably, since the number of particles decreases as the size of the model decreases, the particle curtain of the scaled model appears more dispersed than in the physical model. However, by observing the distribution of red and blue, it can be seen that there are subtle deviations in the mix effects of particles in different models. It should be noted that this study has examined only the force similarity of single particles to derive the relationship between the gravitational acceleration and the rotational speed of scaled models, without considering the influence of the contact between particles. Thus, our conclusion is feasible for single particles by changing the rotational speed and gravitational acceleration, and it is also feasible for the outer boundary of the multi particles during the throwing process. Since we concentrate on the particles in the process of throwing, only the profiles of the particle curtains in different models are extracted and compared as shown in Fig. 12 (For simplicity, it only shows the second, fourth, sixth, and seventh particle curtains when the rotation angle is 8 rad). From Figs. 12b and c, the upper end contour of the particle curtain fits well and the lower end has a normal deviation due to more dispersed particles. To further illustrate the gain of computational efficiency by implementing the similarity approach, the calculation time of each simulation is counted and listed in Table 10. All the simulations are carried out on a Dell PowerEdge T620 workstation with an Inter (R) Xeon (R) CPU E5-2643 of 3.30 GHz and a RAM of 96.0 GB.

Table 10 Calculation time of each simulation.

	Physical model	Scaled model 1	Scaled model 2	Scaled model 3	Scaled model 4	Scaled model 5
Radius of mill (m)	3.9	3.6	3.3	3.0	2.3	1.5
Total mass of particles (kg)	2.06×10^4	1.62×10^4	1.34×10^4	8.97×10^3	4.49×10^3	1.19×10^3
Total number of particles	231461	182022	150562	100786	50449	13370
Elapsed computation time (hours)	35.20	25.60	11.10	10.50	7.05	0.65

To further verify the formula proposed above, a particle mass flow monitoring box is established at the same position of the physical model and the scaled models, and the size of the box is equal to the size of the groove between two adjacent lifters, as shown in Fig. 13 In each model, the mass of the particles in the monitoring box is measured at different times and divided by the total mass of particles. The chart of mass flow monitoring is obtained via statistical comparison, as shown in Fig. 14. From the mass flow monitoring curve, the particle flow trends in the physical model and the scaled models are almost identical.

5. Conclusions and future work

The relationship between the detaching angle of the particle and the radius of the ball mill, the rotational speed of the mill and the gravitational acceleration is investigated by analysing the force balance of a single particle at the moment of detachment from the mill wall. The DEM models of particle movement in ball mills with different radii are developed, and the detaching angles remain similar by changing the rotational speed of the mill and the gravitational acceleration. From the aspects of the motion trajectory of a single particle and the energy change, the above equation is verified, and the following conclusions are obtained:

(1) In DEM simulations, if the system is too large to model according to the actual size of 1:1, the influence of the model or particle size on the accuracy of the simulation results must be evaluated.

(2) To reduce the computational scale of the simulation and improve the computational efficiency, methods that reduce the size of the model and change the particle size can be used. However, the simulation of the kinematic parameters (such as rotational speed) or physical parameters (such as gravitational acceleration) must be calibrated.

(3) To ensure that the particle detaching angles in scaled models are identical, the rotational speed of the mill in the scaled model needs to be increased to $\sqrt{S}$ times that of the physical model if the gravitational acceleration is kept constant. The energy change of the particle throwing process in the scaled model is 1/S times of the physical model. If the rotational speed of the mill is kept constant, the gravitational acceleration in the scaled model needs to be decreased to 1/S times that of the physical model, and the energy change in the particle throwing process in the scaled model is $1/S^2$ times of the physical model.

The present similarity approach of particle force balance produces well consistent simulation results in the single-particle system, and it also well captures the falling process of the multiple-particle system. By changing the rotational speed and gravitational acceleration to reduce the simulation system, the calculation speed and efficiency are much improved. However, it should be noted that the interactions between particles need to be considered in the multiple-particles systems in the future, especially in the performance of particle mixing. Further study of the similarity

of the particle contact characteristics is necessary to make the mixing process of the particles consistent with the physical model.

Nomenclature

R	radius of ball mill (mm)
R^P	radius of the physical model (mm)
R^S	radius of the scaled model (mm)
α	detaching angle (°)
α^P	detaching angle in the physical model (°)
α^S	detaching angle in the scaled model (°)
ω	rotational speed of mill (rad/s)
ω^P	rotational speed of mill in the physical model (rad/s)
ω^S	rotational speed of mill in the scaled model (rad/s)
F	centrifugal force (N)
m	mass of the particle (kg)
g	gravitational acceleration (m/s^2)
g^P	gravitational acceleration in the physical model ($m/s^{2)}$
g^S	gravitational acceleration in the scaled model ($m/s^{2)}$
S	scaled coefficient
v_a, v_b	velocity of any two point between t_1-t_5 (m/s)
h_a, h_b	height of any two point between t_1-t_5 (m)
h_a^P, h_b^P	height of any two point between t_1-t_5 in the physical model (m)
h_a^S h_b^S	height of any two point between t_1-t_5 in the scaled model (m)
$\lvert\Delta E\rvert$	energy change (J)
$\lvert\Delta E\rvert^P$	energy change in the physical model (J)
$\lvert\Delta E\rvert^S$	energy change in the scaled model (J)
λ_1, λ_2	scale factor
F_i	out-of-balance force component of the particle
M_i	unbalanced moment component caused by contact force (N/m)
ω_i	rotational speed of particle (rpm)

I	rotational inertia of the particle ($kg \cdot m^2$)
β_g	global damping coefficient
dt	time step (s)
V_i	translational velocity (m/s)
K_n	normal spring stiffness constant
K_t	tangential spring stiffness constant
C_n	normal damping coefficient
C_t	tangential damping coefficient
E^*	equivalent Young's Modulus
E_a, E_a	Young's Modulus of contact element a and b
γ_a, γ_b	Poisson ratio of contact element a and b
R_a, R_a	radius of contact element a and b
m^*	equivalent mass
β	damping ratio
S_n	normal stiffness
m_a, m_b	mass of contact element a and b
e	coefficient of restitution
$\overline{v_n^{rel}}$	normal relative velocity between contact element a and b
δ_t	tangential overlap
S_t	tangential stiffness
G^*	equivalent shear modulus
G_a, G_b	shear modulus of contact element a and b
$\overline{v_t^{rel}}$	tangential relative velocities between contact element a and b
μ_s, μ_r	coefficient of static and rolling friction
R_i	radius of particle (mm)
ρ_i	density of particle (kg/m^3)
η	filling rate
T	time of simulation (s)
n	porosity

υ	poison ratio
G	shear modulus (pa)
ρ_d	density of mill (kg/m^3)
μ_1, μ_2	coefficient of static friction of particle-particle and particle-wall
m_{r1}, m_{r2}	coefficient of rolling friction of particle-particle and particle-wall
e_1, e_2	restitution coefficient of particle-particle and particle-wall

Acknowledgement

This work was supported by the National Natural Science Foundation of China (Grant No. 51605409, 11772135, 51606040 and 51475402)

References

[1] P.A. Cundall, O.D.L. Strack, A discrete numerical model for granular assemblies, Geotechnique. 29 (1979) 47-65.

[2] Y. Chen, L.J. Munkholm, T. Nyord, A discrete element model for soil-sweep interaction in three different soils, Soil. Till. Res. 126 (2013) 34-41.

[3] M. Jiang, Y. Dai, L. Cui, B. Xi, Experimental and DEM analyses on wheel-soil interaction, J. Terramechanics, 76 (2017) 15-28.

[4] W. G. Shen, T. Zhao, G. B. Crosta, F Dai, Analysis of impact-induced rock fragmentation using a discrete element approach, Int. J. Rock Mech. Min, 98 (2017) 33-38.

[5] S. Pantaleev, S. Yordanova, A. Janda, M. Marigo, An experimentally validated DEM study of powder mixing in a paddle blade mixer, Powder Technol. 311 (2017) 287-302.

[6] T.I. Zohdi, Modeling and efficient simulation of the deposition of particulate flows onto compliant substrates, Int. J. Eng. Sci. 99 (2016) 74-91.

[7] H. Tangri, Y. Guo, J.S. Curtis, Packing of Cylindrical Particles: DEM Simulations and Experimental Measurement, Powder Technol. 317 (2017) 72-82.

[8] S. Jiang, X. Li, Y. Tan, H. Liu, Z. Xu, R. Chen, Discrete element simulation of SiC ceramic with pre-existing random flaws under uniaxial compressio, Ceram. Int. 43 (2017) 13717-13728.

[9] Y. Tan, D. Yang, Y. Sheng, Discrete element method (DEM) modeling of fracture and damage in the machining process of polycrystalline SiC, J. Eur. Ceram. Soc. 29 (2009) 1029-1037.

[10] S. Jiang, X. Li, L. Zhang,Y. Tan, R. Peng, R. Chen, Discrete element simulation of SiC ceramic containing a single pre-existing flaw under uniaxial compression, Ceram. Int. 44 (2017) 3261-3276

[11] S. Zhou, H. Zhu, Z. Yan, J. W. Ju, L. Zhang, A micromechanical study of the breakage mechanism of microcapsules in concrete using PFC2D, Constr. Build. Mater. 115 (2016) 452-463.

[12] J.D. Riera, L.F.F. Miguel, I. Lturrioz, Evaluation of the discrete element method (DEM) and of the experimental evidence on concrete behaviour under static 3D compression, Fatigue. Fract. Eng. M. 39 (2016) 1366-1378.

[13] Y.T. Feng, D.R.J. Owen, Discrete element modelling of large scale particle systems—I: exact scaling laws, Comput. Mech. 1 (2014) 159–168.

[14] G.J. Finnie, N.P. Kruyt, M. Ye, C. Zeilstra, J. A. M. Kuipers, Longitudinal and transverse mixing in rotary kilns: A discrete element method approach, Chem. Eng. Sci. 60 (2015) 4083-4091.

[15] Y. L. Ding, R. N. Forster, J. P. K. Seville, D. J. Parker, Scaling relationships for rotating drums, Chem. Eng. Sci. 56 (2001) 3737-3750.

[16] S. Siiria, J. Yliruusi, DEM simulation of influence of parameters on energy and degree of mixing, Particuology. 04 (2011) 406-413.

[17] P. W. Cleary, R. D. Morrison, Comminution mechanisms, particle shape evolution and collision energy partitioning in tumbling mills, Miner. Eng. 86 (2016) 75-95.

[18] F. Geng, L. Gang, Y. Wang, Y. Li, Z. Yuan, Numerical investigation on particle mixing in a ball mill, Powder Technol. 292 (2016) 64-73.

[19] M. H. Wang, R. Y. Yang, A. B. Yu, DEM investigation of energy distribution and particle breakage in tumbling ball mills, Powder technol. 223 (2012) 83-91.

[20] P. Y. Liu, R. Y. Yang, A. B. Yu, DEM study of the transverse mixing of wet particles in rotating drums, Chem. Eng. Sci. 86 (2013) 99-107.

[21] X. Bian, G. Wang, H. Wang, S. Wang, W. Lv, Effect of lifters and mill speed on particle behavior torque and power consumption of a tumbling ball mill: Experimental study and DEM simulation, Miner. Eng. 105 (2017) 22-35.

[22] N. S. Weerasekara, L. X. Liu, M. S. Powell, Estimating energy in grinding using DEM modelling, Miner. Eng. 85 (2016) 23-33.

[23] M. J. Metzger, B. J. Glasser, Simulation of the breakage of bonded agglomerates in a ball mill, Powder technol. 237 (2013) 286-302.

[24] M. S. Powell, N. S. Weerasekara, S. Cole, R. D. LaRoche, J. Favier, DEM modelling of liner evolution and its influence on grinding rate in ball mills, Miner. Eng. 24 (2011) 341-351.

[25] H. Qi, J. Xu, G. Zhou, F. Chen, W. Ge, J. Li, Numerical investigation of granular flow similarity in rotating drums, Particuology. 22 (2015) 119-127.

[26] J. Xu, H. Qi, X. Fang, L. Lu, W. Ge, X. Wang, J. Li, Quasi-real-time simulation of rotating drum using discrete element method with parallel GPU computing, Particuology. 9 (2011) 446-450.

[27] J.Q. Gan, Z.Y. Zhou, A. B. Yu, A GPU-based DEM approach for modelling of particulate systems, Powder Technol. 301 (2016) 1172-1182.

[28] Y. Shigeto, M. Sakai, Parallel computing of discrete element method on multi-core processors, Particuology. 09 (2011) 398-405.

[29] A. Maknickas, A. Kačeniauskas, R. Kačianauskas, R. Balevičius, A. Džiugys, Parallel DEM software for simulation of granular media. Informatica. 17 (2006) 207-224.

[30] T. Weinhart, R. Hartkamp, A. R. Thornton, S. Luding, Coarse-grained local and objective continuum description of three-dimensional granular flows down an inclined surface, Phys. Fluids. 25 (2013) 41-47.

[31] F. Wissing, S. Wirtz, V. Scherer, Simulating municipal solid waste incineration with a DEM/CFD method–Influences of waste properties, grate and furnace design, Fuel. 206 (2017) 638-656.

[32] Y. L Ding, R. Forster, J. P. K. Seville, D. J. Parker, Granular motion in rotating drums: bed turnover time and slumping–rolling transition, Powder Technol. 124 (2002) 18-27.

[33] T. Iwasaki, T. Yabuuchi, H. Nakagawa, S. Watano, Scale-up methodology for tumbling ball mill based on impact energy of grinding balls using discrete element analysis, Adv. Powder Technol. 21 (2010) 623-629.

[34] N. Bosso, A. Gugliotta, A. Somà, Simulation of narrow gauge railway vehicles and experimental validation by mean of scaled tests on roller rig, Meccanica. 43 (2008) 211-223.

[35] Y. T. Feng, K. Han, D. R. J. Owen, J. Loughran, On upscaling of discrete element models: similarity principles, Eng. Computation. 26 (2009) 599-609.

[36] F. Pedrayes, J. G. Norniella, M. G. Melero, J. M. Menéndez-Aguado, J. J. D. Coz-Díaz,.Frequency domain characterization of torque in tumbling ball mills using DEM modelling: Application to filling level monitoring, Powder Technol. 323 (2018) 433-444.

[37] P.W. Cleary, Predicting charge motion, power draw, segregation and wear in ball mills using discrete element methods, Miner. Eng. 11 (1998) 1061–1080.

[38] DEM solutions, EDEM V2.7 User Manual. (2015).

[39] A. Di Renzo, F. P. Di Maio, Comparison of contact-force models for the simulation of collisions in DEM-based granular flow codes, Chem. Eng. Sci. 59 (2004) 525–541.

List of figure captions:

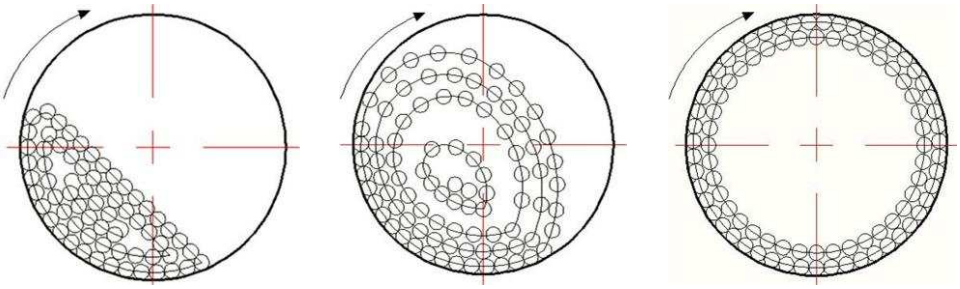

(a) Slipping (b) Cataracting (c) Centrifuging

Fig. 1. Schematic diagram of the material movement in the ball mill [33].

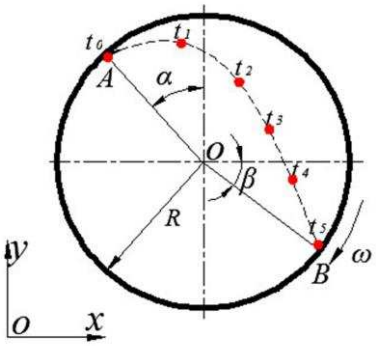

Fig. 2. Motion trajectory of a particle in the outermost layer of the mill.

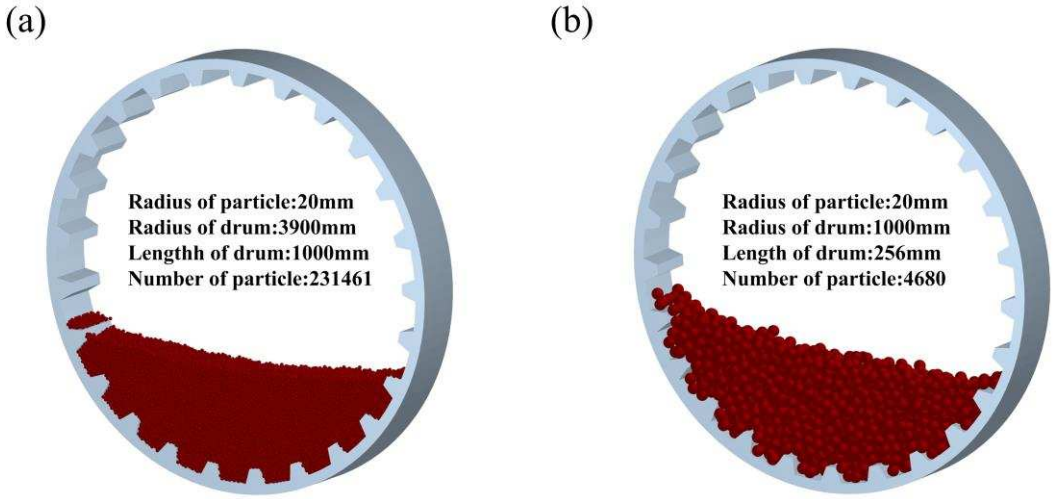

Fig. 3. (a) Particles in the physical model; (b) particles in the scaled model.

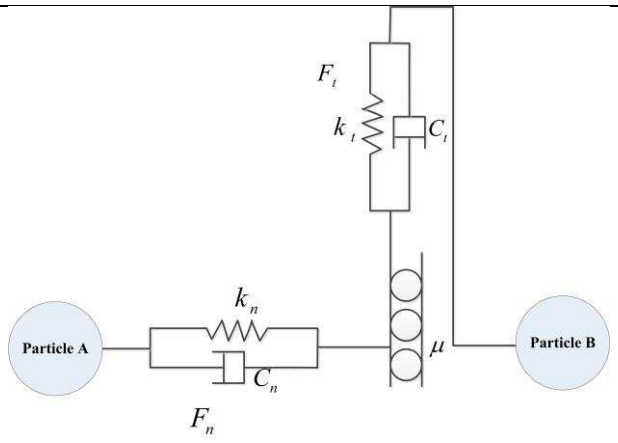

Fig. 4. Contact model of ball-ball.

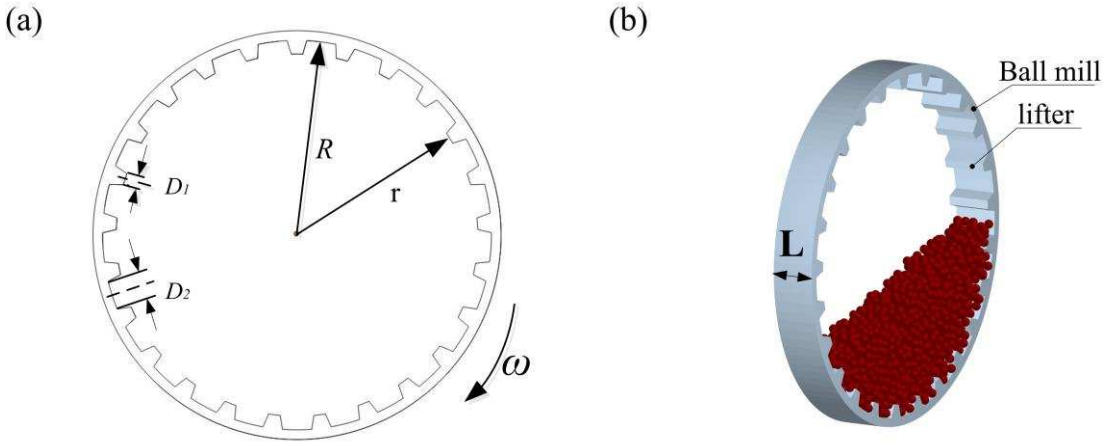

Fig. 5. (a) Schematic diagram of the ball mill; (b) DEM model of the ball mill.

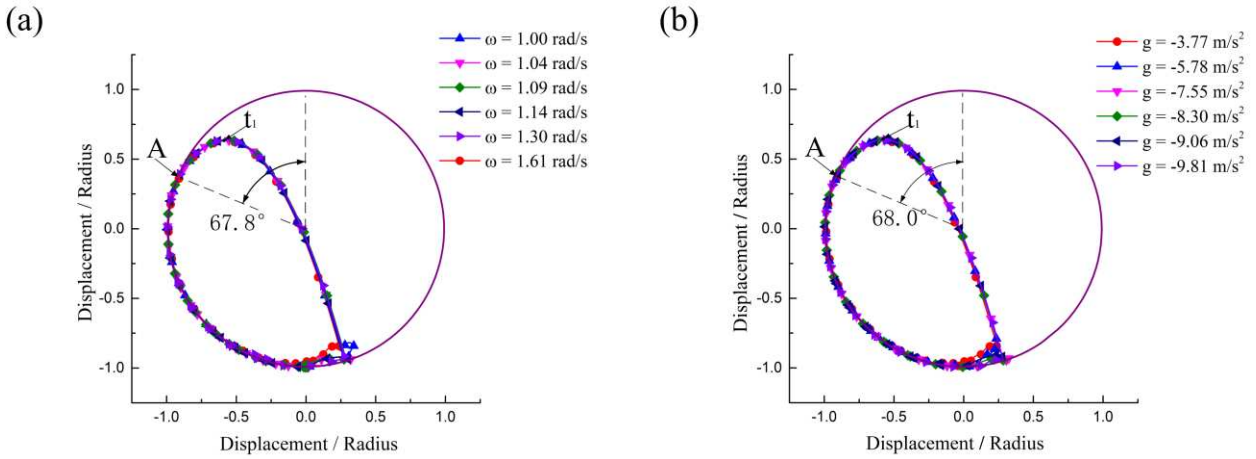

Fig. 6. Motion trajectories of particle in two schemes: (a) change rotational speed of the mill; (b) change the gravitational acceleration.

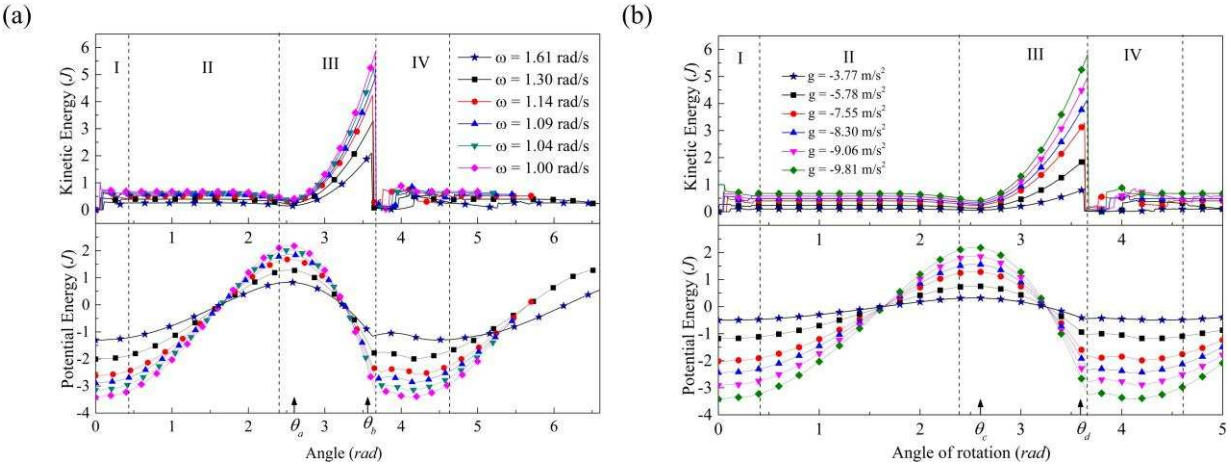

Fig. 7. (a) Energy change at different rotational speeds of mill (g=9.81 m/s^2); (b) Energy change at different gravitational acceleration (ω=1 rad/s).

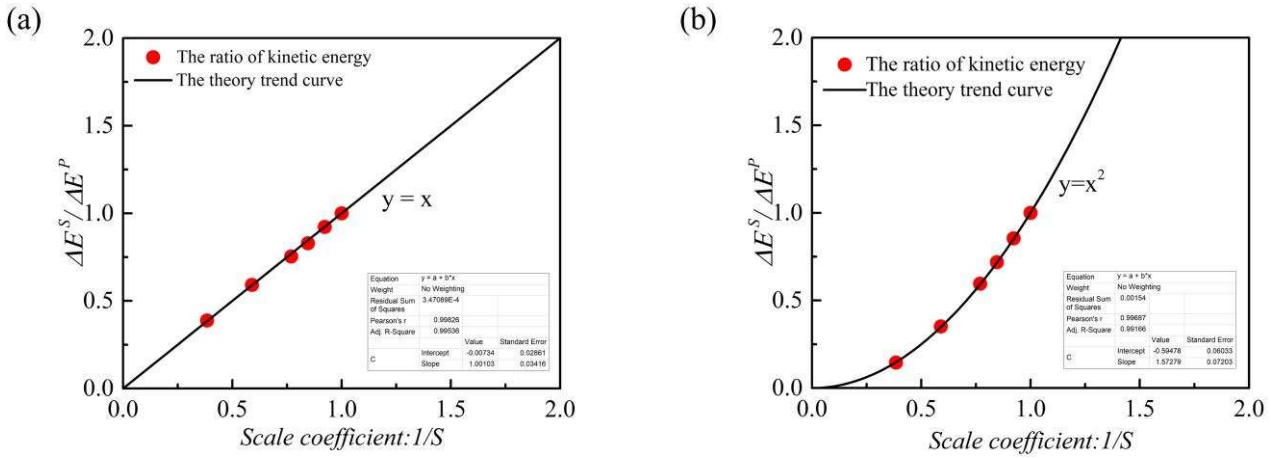

Fig. 8. Ratio of energy changes in two schemes: (a) change the rotational speed of the mill; (b) change the gravitational acceleration.

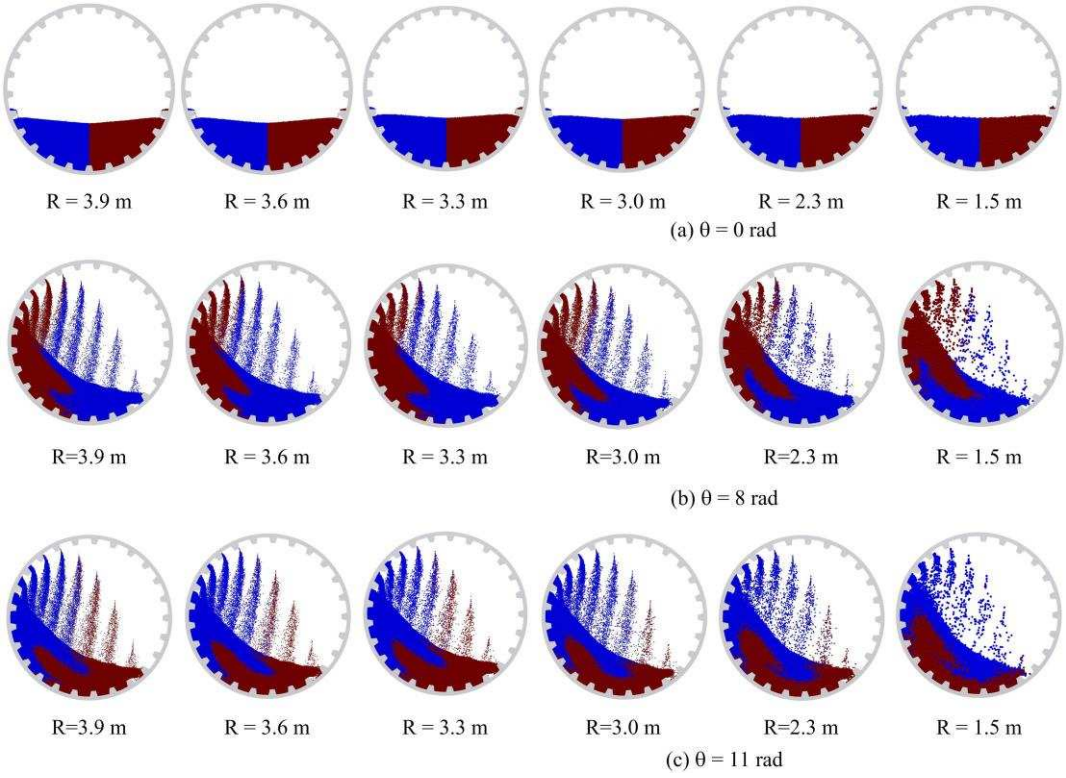

Fig. 9. Particle motion patterns in the physical model and the scaled model at different rotational angles when changing the mill rotational speed.

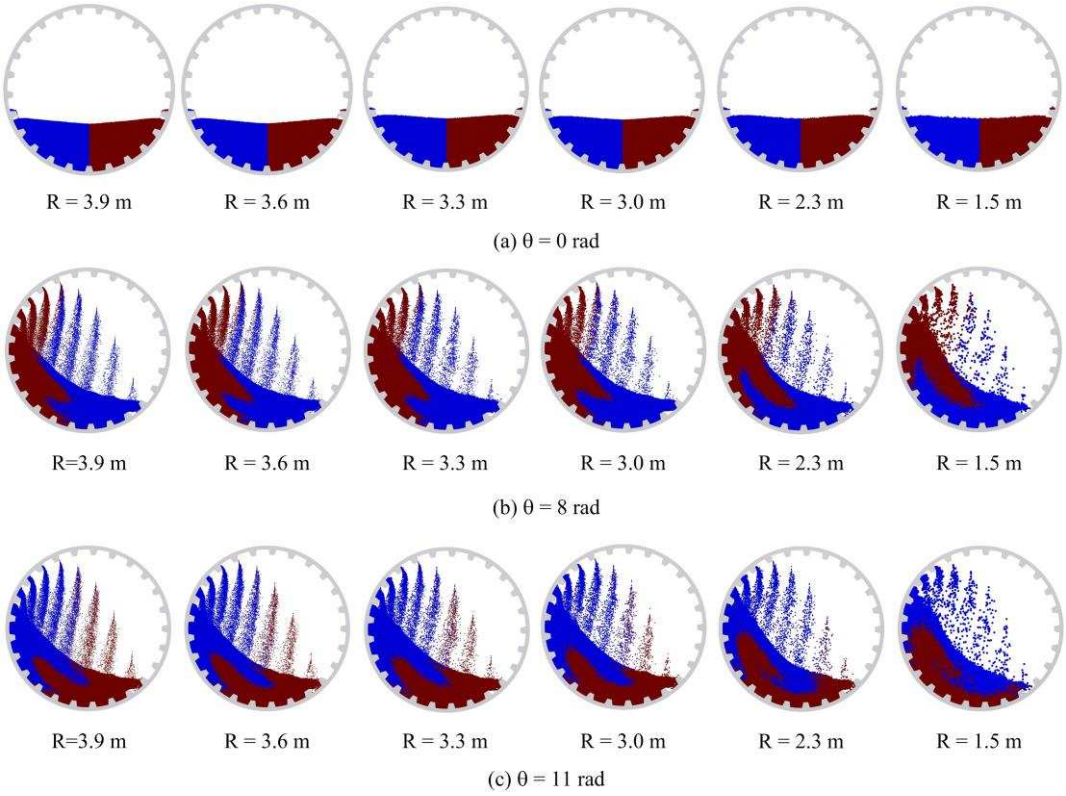

Fig. 10. Particles motion patterns in the physical model and the scaled model at different rotational angles when changing the gravitational acceleration.

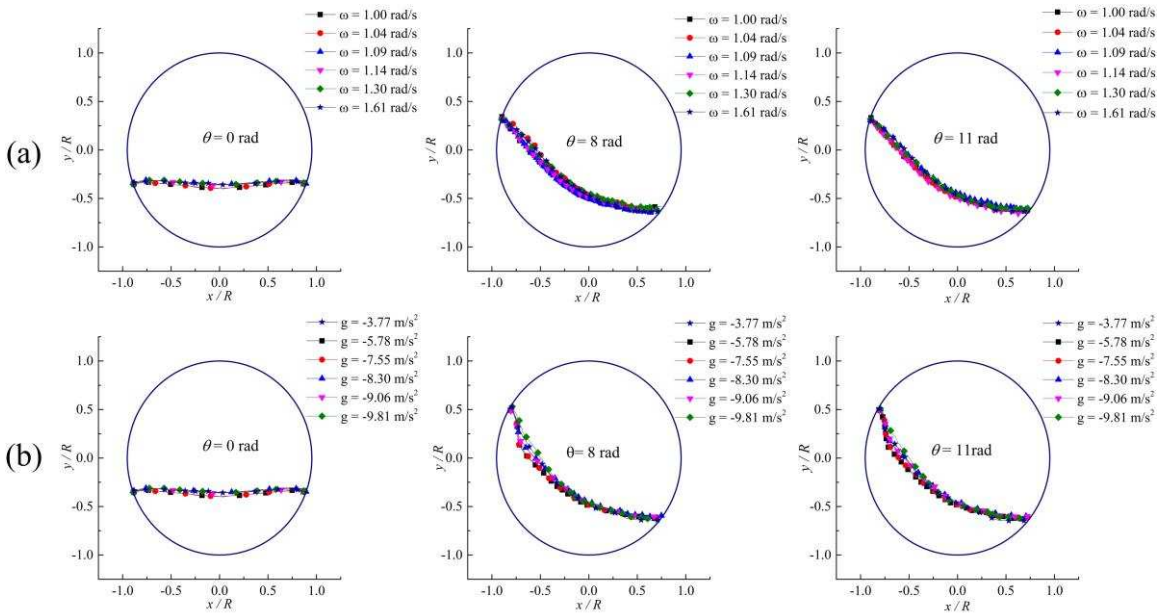

Fig. 11. Schematic diagram of the evolution of the overall surface profiles of particles in the ball mill: (a) change the rotational speed of the mill; (b) change the gravitational acceleration.

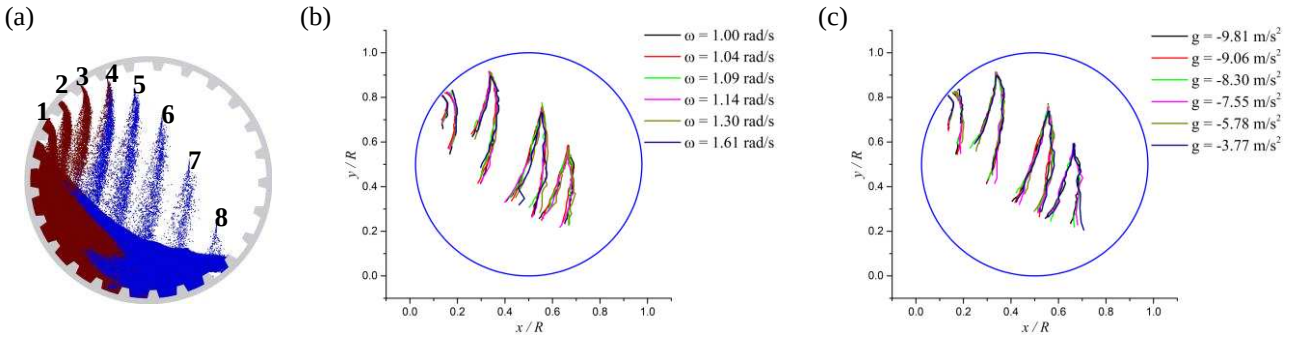

Fig. 12. The contour of the particle curtain (a) Particle curtain number; (b) change the rotational speed of ball mill; (c) change the gravitational acceleration.

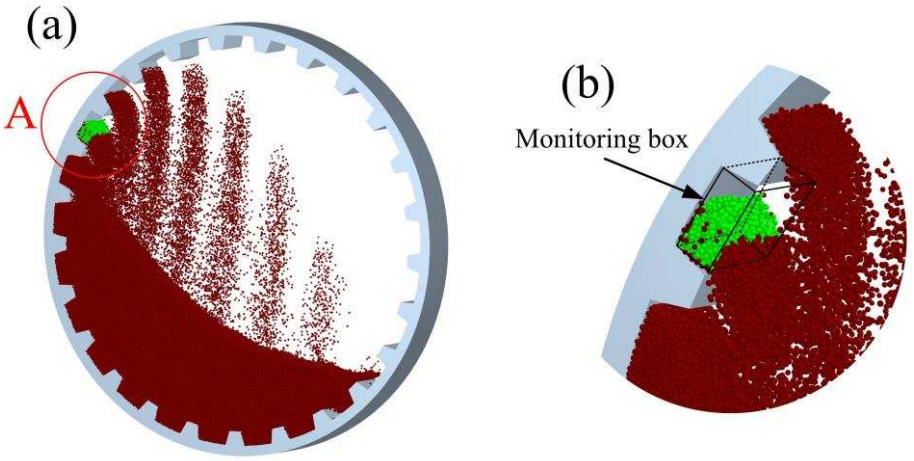

Fig. 13 (a) Monitoring box in the ball mill; (b) red circle "A" in the enlarged view.

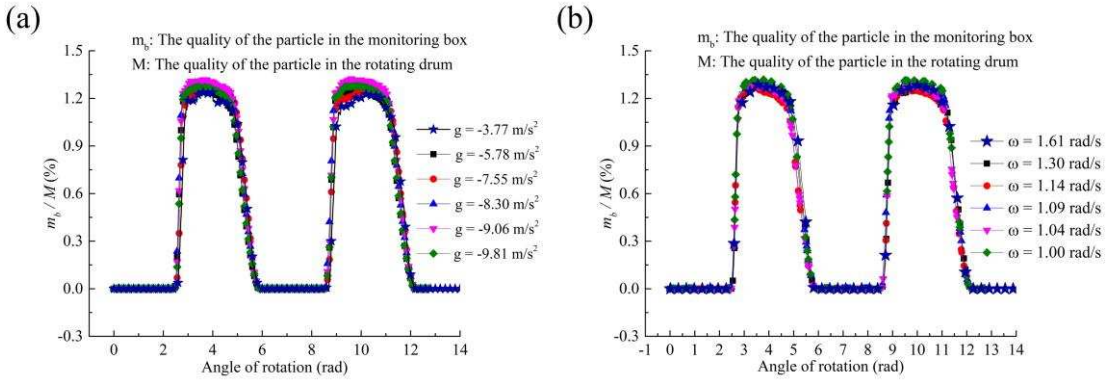

Fig. 14. Flow monitoring results for mills with different radii: (a) change the rotational speed of the mill; (b) change the gravitational acceleration.